Coherent Simulation of Sea-Clutter for a Scanning Radar

Luke Rosenberg
Defence Science and Technology Group
AUSTRALIA
luke.rosenberg@dsto.defence.gov.au

Simon Watts
University College London
UNITED KINGDOM
simon.watts@ucl.ac.uk

ABSTRACT

Future maritime patrol aircraft will often be required to operate at higher altitudes where the clutter return will be stronger, due to the increased grazing angles. One approach to improving target detection performance in this scenario is to exploit coherent processing with a multi-phase centre radar. This paper tackles the problem of producing a realistic simulation of the sea-clutter backscatter which contains the desired amplitude and correlation statistics and provides a range varying Doppler spectrum. Two methods of simulation are presented: a single channel version which is quick to implement and an alternate version suitable for a linear array with multiple receive channels. All parameters used in the simulation are determined by empirical models which in turn rely on user defined inputs including sea state, the wind and swell direction and the grazing angle.

1.0 INTRODUCTION

Traditional maritime patrol aircraft fly at low altitudes to best detect small targets. This operational requirement is now changing with the desire to perform the same mission from higher altitudes. However, when operating at higher grazing angles, the clutter return increases in intensity and reduces the performance that can be achieved by traditional non-coherent detection methods. To recover the performance achieved at lower grazing angles, we now need to consider alternative detection schemes that exploit coherent processing and multi-phase centre techniques such as space time adaptive processing (STAP) [1, 2]. The key to the development of any new detection method is the ability to test results against either real or simulated sea-clutter. Since the former is not always available, this paper presents a comprehensive method for simulating sea-clutter as it would appear from a single or multi phase centre scanning radar.

Over the past years, there has been a lot of work improving sea-clutter modelling techniques to improve the realism of simulated sea-clutter and develop new coherent detection techniques. These are based on the compound Gaussian model with the simulation utilising the memoryless nonlinear transform to generate random samples with a desired amplitude distribution and correlation [3], [4]. Using this technique, Davidson [5] provides a method for generating non-stationary coherent sea-clutter with desired distribution shape and intensity distribution in the Doppler domain. However the method cannot be used to simulate the large magnitude sea-spikes present in the sea-clutter and there is no direct linkage between the time and frequency domains.

A model that can represent the time-varying nature of Doppler spectra in sea clutter was originally described by Watts [6]. For sea clutter with grazing angles $< 2°$, it was observed that the mean Doppler shift of the power spectrum was strongly correlated with the local intensity of the clutter return. This model can be used to simulate time or range-varying Doppler spectra [6–8] and to analytically investigate the performance of signal processing techniques [9]. The most recent work in [7, 10] has extended this modelling to a wider range of sea clutter data gathered by the Defence Science and Technology (DST) Group Ingara radar. An important feature of this data is that it is gathered at higher grazing angles than [6], covering $15°$ to $45°$. In this recent work, the original model was also extended to include a bimodal form to better capture sea-spikes which may be present. A comprehensive parameter model was also presented which could relate a desired sea-state, grazing angle and wind and swell direction to produce the required model parameters.

In Section 2, details of the collection geometry, the evolving Doppler spectrum model and the simulation method are presented. This is related to the work presented in [11], but goes further by allowing for a generic antenna pattern and relaxing the requirement for a fixed coherent processing interval (CPI) when generating the data. Extensions are also shown for improved sea-spike modelling using a bimodal spectrum and how the simulation method can be altered to model a radar with multiple-phase centres. Section 3 then provides examples for both simulation methods with the key parameters measured to verify the simulation accuracy.

2.0 SCANNING RADAR SIMULATION

The scanning airborne radar scenario is shown in Fig. 1 with the radar platform travelling with velocity v_p and the radar look direction at an angle θ_{plat} relative to the platform motion. The angle between the radar look direction and the wind is given by ψ.

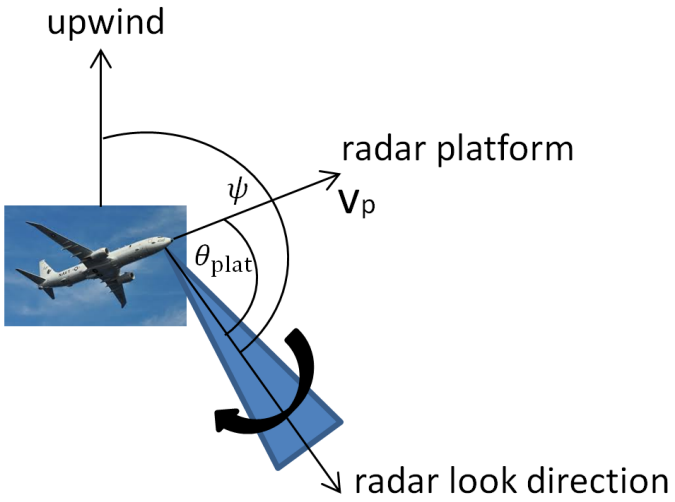

Figure 1: Scanning airborne radar scenario.

As the radar scans with a rate ω_{scan}, there are $N_p = f_r/\omega_{\text{scan}}$ pulses in a given scan, where the pulse repetition frequency (PRF) of the radar is f_r. Also, if the two-way azimuth 3 dB beamwidth is ϕ_{3dB}, then a point target will be in the beam for $T_{\text{targ}} = \phi_{3dB}/\omega_{\text{scan}}$ seconds or $N_{\text{targ}} = \text{floor}\left(T_{\text{targ}} f_r\right)$ pulses. This limit determines the number of pulses which can be used for coherent processing.

2.1 Evolving Doppler spectrum model

The evolving Doppler model forms the basis of the simulation technique presented in this paper. As outlined in [3, 6], it describes a Gaussian shaped spectrum,

$$G_0(f,\tau,s,\mathbf{\Omega}) = \frac{\tau}{\sqrt{2\pi}s(\mathbf{\Omega})}\exp\left[-\frac{(f-m_{\text{f}}(\tau,\mathbf{\Omega}))^2}{2s(\mathbf{\Omega})^2}\right] \tag{1}$$

where τ is the normalised underlying mean or texture and the set $\mathbf{\Omega} \equiv \{\theta_{\text{plat}},\psi,\theta_{\text{swell}},U,H_{1/3}\}$ represents the variables used to characterise the model parameters, θ_{swell} is the angle between the wind and swell, U is the wind speed and $H_{1/3}$ is the significant wave height. The spectral width, s of the clutter is a Gaussian random variable with mean s_{mean} and standard deviation, s_{std}, while the mean Doppler frequency, $m_{\text{f}}(\tau,\mathbf{\Omega})$ is given as

$$m_{\text{f}}(\tau,\mathbf{\Omega}) = A(\mathbf{\Omega}) + B(\mathbf{\Omega})\tau + f_{\text{plat}} \tag{2}$$

where A and B relate the centre point with the texture. The third term accounts for the Doppler shift due to the moving platform [2],

$$f_{\text{plat}} = \frac{2v_p}{\lambda} \cos\theta_{\text{plat}} \tag{3}$$

where λ is the radar wavelength. This frequency offset can be significant when the radar is forward looking ($\theta_{\text{plat}} = 0$), while it is zero when the radar is side looking ($\theta_{\text{plat}} = \pi/2$). Therefore, when analysing a CPI from an arbitrary look angle, one of the first processing steps required is to estimate and correct for the Doppler centroid using a technique such as the wavelength diversity algorithm [12].

Finally, the underlying Doppler spectrum will also be broadened by the azimuth two-way beampattern, $A(\theta)$, which is maximum when azimuth angle, $\theta = 0$ and can be written in terms of frequency with $f = 2v_p \sin\theta/\lambda$. There are a few ways this can be included in the modelling. For the single channel simulation method, the beampattern is explicitly included by the convolution,

$$G(f, \tau, s, \mathbf{\Omega}) = A(f) * G_0(f, \tau, s, \mathbf{\Omega}). \tag{4}$$

An alternative method described in Section 2.4 is required when simulating the return from multiple phase centres. This technique modulates the clutter sub-patches with the antenna beampattern, but is more computationally intensive.

2.2 Simulation method

The implementation of the simulation is based on a convolution of the desired clutter impulse response g and the compound Gaussian signal model, $x\sqrt{\tau}$, where x are random complex normal variates. The filter at pulse index m is given by [3],

$$y(m, \tau) = \left(\frac{1}{\sqrt{2}}\right) \sum_{n=-N/2}^{N/2} g(n, \tau, s, \mathbf{\Omega}) x(m+n) \sqrt{\tau(m+n)}, \tag{5}$$

where N is the filter order. The discretised clutter impulse response, g is found by taking the Fourier transform of (4) and is given as,

$$g(n, \tau, s, \mathbf{\Omega}) = A(n/f_r) \exp\left[-j \frac{m_{\text{f}}(\tau, \mathbf{\Omega}) 2\pi n}{f_r}\right] \exp\left[-(2\pi s(\mathbf{\Omega}) n f_r)^2\right]. \tag{6}$$

The output of this convolution represents the return for a single pulse and hence this technique can be implemented by repeating (5) for each pulse in the scan (i.e. as a sliding window) with the parameters of $\mathbf{\Omega}$ updated at each iteration. This makes the technique suitable for implementation in real time system. Alternatively, we can just specify a block of pulses, N_b to be generated at a desired look angle.

For this implementation to work, the normalised texture must be approximately constant over the desired observation period. However, this is only approximately true as it changes when the radar scans to different look directions. To ensure the compound model holds, but the variation of the normalised texture exists for different scanning locations, the simulation is implemented over two stages.

1. The first stage simulates the normalised texture, τ over the entire scan, but for only a small number of positions, $M \approx 10$. At each position, the texture is simulated with the correct statistical distribution and range correlation. The distribution shape and correlation length are determined using the user defined input parameters (sea state, wind and swell direction direction, grazing angle) as inputs to the empirical parameter models [7]. The small number of positions makes sure that the texture does not vary significantly over the integration time of the filter. The number of range samples, N_r is a user input and hence the texture has size $M \times N_r$. After this processing step is completed, the texture is then interpolated to the correct time scale, $1/f_r$, using a spline for accuracy and has size $N_p \times N_r$.

2. For the second stage, realisations of the speckle random variable, x and the spread, s are generated for each desired pulse and range bin. The speckle has a complex normal distribution with zero mean and variance $1/\sqrt{2}$, while the spread initially has a normal distribution with zero mean and unity variance. This signal is later offset and scaled with the correct s_{mean}, s_{std}. If we consider a block of N_b pulses, then the size of these variables are $N_b \times N_r$.

   For each pulse, the correct block of texture data of size $N \times N_r$ is extracted and the parameters, A, B, s_{mean}, s_{std} are derived using the empirical models in [7]. The spread is now offset and scaled and the clutter impulse response formed from (6). Filtering is then performed using (5) with the result normalised to have unity mean power. Additive thermal noise is then added to ensure the correct clutter to noise ratio (CNR).

2.3 Modelling sea-spikes

To improve the fidelity of the sea-spike representation, we can replace the model in (1) with the bimodal spectrum presented in [7,10] and replace the mean Doppler offset, $m_{\text{f}}(\tau, \mathbf{\Omega})$ will its equivalent bi-model version. This Gaussian mixture model uses a ratio, β, to determine how much of each Gaussian component is present,

$$G_{\text{bi}}(f, \tau, s, \mathbf{\Omega}) = (1 - \beta) G_0(f, \tau, s_1, \mathbf{\Omega}) + \beta G_0(f, \tau, s_2, \mathbf{\Omega}) \tag{7}$$

where s_1 and s_2 are the Doppler spreads for each component. If there are discrete scatterers in the scene from a target or persistent sea-spike, there will be an extra spread in the Doppler spectrum due to the scanning motion of the radar which can be modelled by

$$s_{\text{scan}} = \frac{\sqrt{2 \ln 2}}{2\pi} \frac{\omega_{\text{scan}}}{\phi_{3dB}}. \tag{8}$$

If we consider the second Gaussian in the model as representing the sea-spike component, then the Doppler spread for the first component, $s_1(\mathbf{\Omega}) = s(\mathbf{\Omega})$ and the second component is

$$s_2(\mathbf{\Omega}) = \sqrt{s_1^2(\mathbf{\Omega}) + s_{\text{scan}}^2}. \tag{9}$$

Implementation of this model is similar to the original with the appropriate bimodal parameter models used from [7].

2.4 Multiple phase centres

Modelling the return from multiple phase centres requires the representation of clutter sub-patches with the return from the antenna beampattern dictating the energy received in each direction. This is shown in Fig. 2 for a 2 phase centre system with spacing D between phase centres. The implementation requires the texture to be broken up into K sub-patches so that

$$\sum_{k=1}^{K} \tau_k = \tau \tag{10}$$

where the texture return for the k^{th} patch, $\tau_k = A(f_k)\tau$, models the return from the appropriate part of the beam. With this change, the convolution of the beampattern can be removed from (4) so that the spectrum model is now G_0 (or G_{bi}) instead of G. This also requires redefining the platform centre frequency as

$$f_{\text{plat},k} = \frac{2v_p}{\lambda} \cos(\theta_{\text{plat}} - \theta_k) \tag{11}$$

with the overall return from the l^{th} sub-aperture given by

$$\tilde{y}_l(m) = \sum_{k=1}^{K} y(m, \tau_k) \exp\left(\frac{j2\pi}{\lambda}\left(R_{k,l} - R_{k,1}\right)\right)$$
$$\approx \sum_{k=1}^{K} y(m, \tau_k) \exp\left(\frac{j2\pi}{\lambda} D(l-1)\sin\theta_k\right) \quad (12)$$

where the approximation assumes a linear array with backscatter from the far field. This implementation is clearly more computationally intensive than the single channel model due to the extra summation. However, the range of sub-patches which contribute to the sum in (12) can be reduced by only including those where $A(f_k) > \epsilon$, where $\epsilon \approx 10^{-3}$.

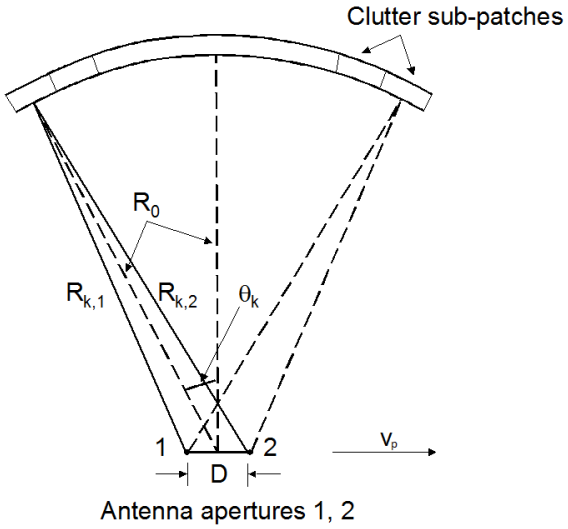

Figure 2: Geometry of clutter sub-patches observed by two phase centres.

3.0 SIMULATION EXAMPLES

In this section, both single and multi-phase centre implementations are demonstrated with the key simulated parameters measured to verify the simulation accuracy. For the following examples, the radar is travelling at 80 m/s and scanning at 5 rpm with a PRF of 3 KHz. The azimuth 3 dB beamwidth is 3° and the centre frequency and bandwidth are 10 GHz and 200 MHz respectively. The radar is scanning in a clockwise direction with the radar platform travelling North with the wind and swell from the West. The bimodal spectrum is used with amplitude probability density function (PDF) modelled with a K-distribution and the filter order, $N = 64$. Other radar, environmental and implementation parameters are given in Table 1. In each example, the Doppler centroid has been estimated and the spectrum centred.

Figures 3 and 4 show the single and multi channel simulated data when the radar is looking forward (crosswind, $\theta = 0°$, $\psi = 270°$) and sidewards (upwind, $\theta = 90°$, $\psi = 0°$). for the latter case, there are $K = 51$ clutter patches and a linear array of $L = 10$ channels has been used with $D = \lambda/2$ spacing between the phase centres. There is clearly more correlation present in the forward looking case due to the narrower Doppler spectrum. Also, while the widths of the forward looking spectra appear slightly different, when averaged over range, they both match the desired value. To verify the accuracy of the simulation, data is generated for each 10° in azimuth and the spatial correlation length, the shape and the spectral width (analogous to the temporal correlation) are measured. Figures 5 and 6 show this comparison for both cases. While there is some fluctuation for the estimates, in general there is a good match between the measured and desired values.

Table 1: Simulated data characteristics.

Radar scan rate	5 rpm
Aircraft speed	80 m/s
Azimuth 3 dB beamwidth (two-way)	3°
Centre frequency	10 GHz
Bandwidth	200 MHz
Pulse repetition frequency	3 KHz
Grazing angle	30°
Sea state	3
No. of pulses a target will be in the beam	300
Amplitude PDF model	K distribution
Spectral model	Bimodal

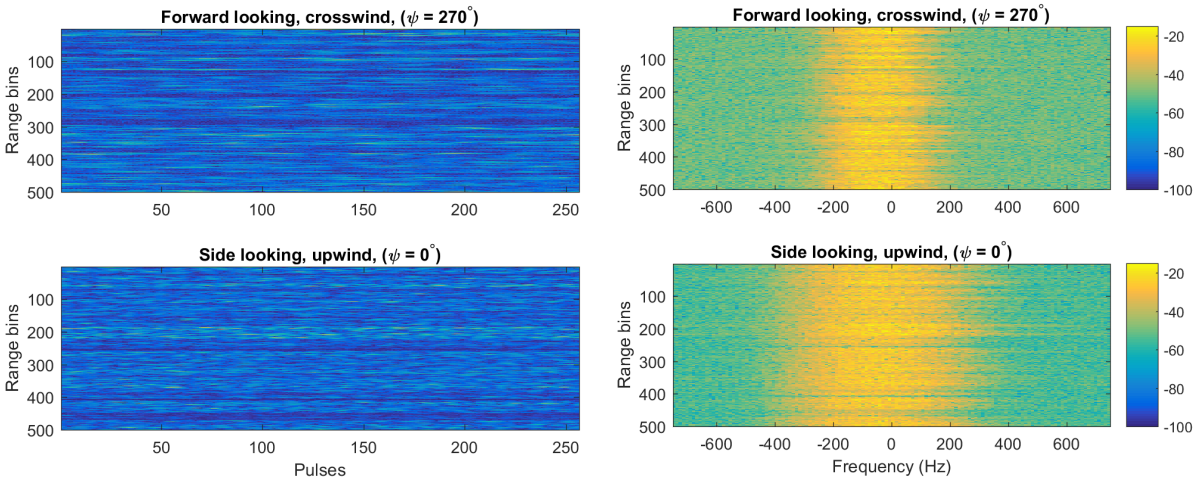

Figure 3: Single channel simulation example with forward and side looking geometries. Left - range / time images, right - corresponding Doppler spectra.

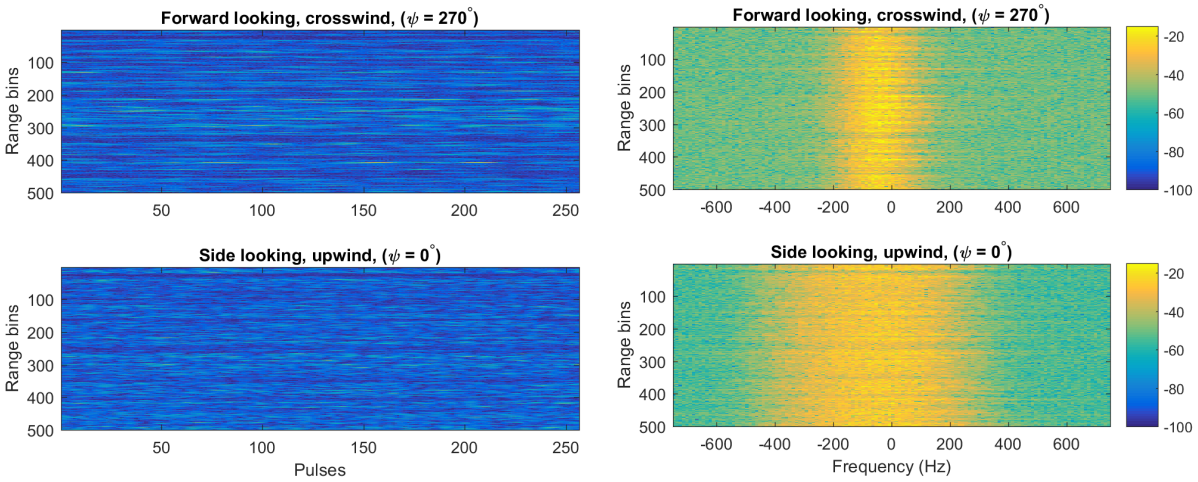

Figure 4: Multi-phase centre simulation example with forward and side looking geometries. Left - range / time images, right - corresponding Doppler spectra.

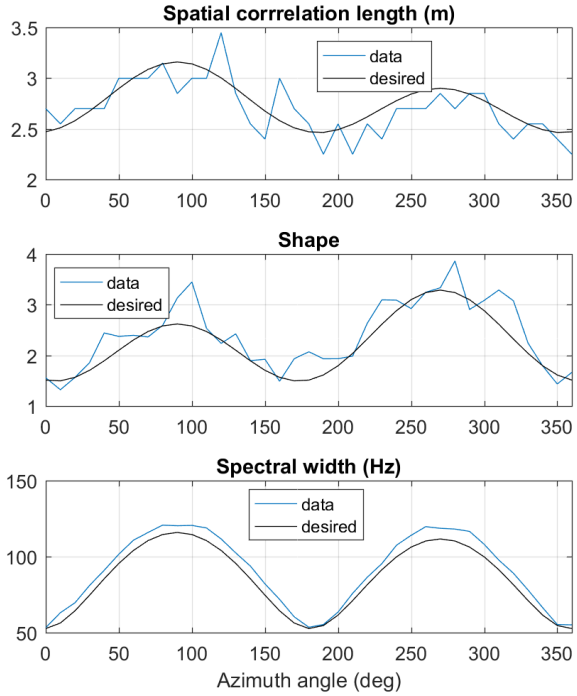

Figure 5: Simulation validation for single-channel implementation.

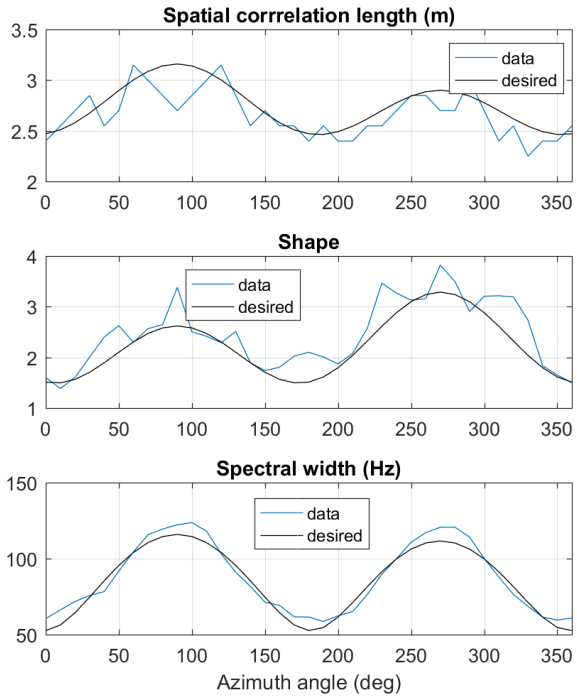

Figure 6: Simulation validation for multi-channel implementation.

To test the multi-channel aspects of the simulation, the Fourier power spectrum and the optimal (minimum variance) spectrum has been calculated for different steering angles. These are calculated as

$$P_F(\theta, f) = \mathbf{v}^H(\theta, f)\hat{\mathbf{R}}\mathbf{v}(\theta, f), \tag{13}$$

$$P_{MF}(\theta, f) = \frac{1}{\mathbf{v}^H(\theta, f)\hat{\mathbf{R}}^{-1}\mathbf{v}(\theta, f)} \tag{14}$$

where the space time steering signal is the Kronecker product,

$$\mathbf{v}(\theta, f) = \mathbf{v}_{\text{spat}}(\theta) \otimes \mathbf{v}_{\text{temp}}(f) \tag{15}$$

of the spatial steering vector with length $L \times 1$

$$\mathbf{v}_{\text{spat}}(\theta) = \frac{1}{\sqrt{2}}\left[v_{\text{spat},1}(\theta, f), v_{\text{spat},2}(\theta, f), \ldots, v_{\text{spat},L}(\theta, f)\right]^T \tag{16}$$

with elements

$$v_{\text{spat},l}(\theta) = \exp\left[j2\pi(l-1)\frac{d}{\lambda}\sin(\theta)\right], \tag{17}$$

and the temporal steering vector of length $C \times 1$

$$\mathbf{v}_{\text{temp}}(f) = \frac{1}{\sqrt{2}}\left[v_{\text{temp},1}(f), v_{\text{temp},2}(f), \ldots, v_{\text{temp},C}(f)\right]^T \tag{18}$$

with elements

$$v_{\text{temp},c}(f) = \exp\left[-\frac{j2\pi(c-1)f}{f_{\text{r}}}\right]. \tag{19}$$

The covariance matrix, $\hat{\mathbf{R}}$ can be estimated by forming the outer product of the space-time vector, $\mathbf{y}_q$ for the q^{th} range bin and then averaging over $2LC$ range bins, excluding the cell under test and guard bands. This space time vector is formed by stacking the L spatial elements of simulated data for each pulse and then stacking C blocks of pulses.

$$\hat{\mathbf{R}} = \sum_{q=1}^{2LC} \mathbf{y}_q \mathbf{y}_q^H. \tag{20}$$

Example power spectrums are shown below in Fig. 7 with $C = 10$ pulses. The optimal power spectrum is much narrower as expected with a diagonal slope indicating the effect of platform motion over the measurement time.

4.0 CONCLUSIONS AND FUTURE WORK

This paper has described a sea clutter simulation method for scanning radars with either single or multiple phase centres. The simulation results have been verified by testing against the desired input parameters and show a close match in all cases.

Further research includes modelling the variation of CNR with range and investigating the impact of the CPI length when determining the underlying parameter models. Also, since the parameter models were based on the Ingara medium grazing angle sea clutter data set, the parameter models are currently limited to a range resolution of 0.75 m. In the future, we would like flexibility is selecting other range resolutions.

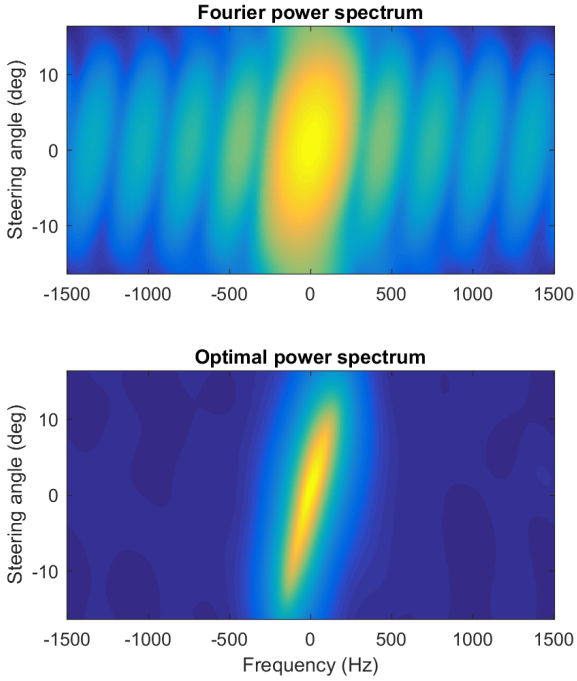

Figure 7: Fourier and optimal power spectrum.

References

[1] L. Rosenberg and S. Watts. Model based coherent detection in medium grazing angle sea-clutter. In *IEEE Radar Conference*, 2016.

[2] R. Klemm. *Principles of Space-Time Adaptive Processing*, volume 21. The Institution of Engineering and Technology, third edition, 2006.

[3] K. D. Ward, R. J. A. Tough, and S. Watts. *Sea Clutter: Scattering, the K-Distribution and Radar Performance*. The Institute of Engineering Technology, second edition, 2013.

[4] S. Bocquet. Simulation of correlated Pareto distributed sea clutter. In *International Radar Conference, Radar 2013*, pages 258–261, September 2013.

[5] G. Davidson. Simulation of coherent sea clutter. *IET Radar Sonar and Navigation*, 4(2):168–177, 2010.

[6] S. Watts. Modeling and simulation of coherent sea clutter. *IEEE Transactions on Aerospace and Electronic Systems*, 48(4):3303–3317, October 2012.

[7] S. Watts, L. Rosenberg, S. Bocquet, and M. Ritchie. The Doppler spectra of medium grazing angle sea clutter; part 2: Exploiting the models. *IET Radar Sonar and Navigation*, 10(1):32–42, 2016.

[8] S. Bocquet, L. Rosenberg, and S. Watts. Simulation of coherent sea clutter with inverse gamma texture. In *International Radar Conference, Radar 2014*, volume TUO.2.5, October 2014.

[9] S. Watts. The effects of covariance matrix mismatch on adaptive CFAR performance. In *International radar conference, Radar 2013*, pages 324–329, September 2013.

[10] S. Watts, L. Rosenberg, S. Bocquet, and M. Ritchie. The Doppler spectra of medium grazing angle sea clutter; part 1: Characterisation. *IET Radar Sonar and Navigation*, 10(1):24–31, 2016.

[11] S. Kemkemian, L. Lupinski, J.-F. Degurse, V. Corretja, R. Cottron, and S Watts. Performance assessment of multi-channel radars using simulated sea clutter. In *International Radar Conference, Radar 2015*, pages 1015–1020, May 2015.

[12] R. Bamler and H. Runge. PRF-ambiguity resolving by wavelength diversity. *IEEE Transactions on Geoscience and Remote Sensing*, 29(6):997–1003, November 1991.